Original Article

CT-guided needle insertion with an optical navigation robot-assisted puncture system: *ex vivo* and *in vivo* experimental studies in the liver and kidneys

Wei Cui[1#], Yi Deng[2#], Jingjing Chen[3], Yanqing Le[3], Huaying Shi[3], Suyi Ye[2], Bingding Huang[4], Xiaoming Chen[1], Jing Li[2,3], Rongde Xu[1]

[1]Department of Interventional Radiology, Guangdong Provincial People's Hospital (Guangdong Academy of Medical Sciences), Southern Medical University, Guangzhou, China; [2]Medical School, Kunming University of Science and Technology, Department of Pulmonary and Critical Care Medicine, The First People's Hospital of Yunnan Province, Kunming, China; [3]Department of Pulmonary and Critical Care Medicine, Guangdong Provincial People's Hospital (Guangdong Academy of Medical Sciences), Southern Medical University, Guangzhou, China; [4]College of Big Data and Internet, Shenzhen Technology University, Shenzhen, China

Contributions: (I) Conception and design: W Cui, Y Deng; (II) Administrative support: R Xu, J Li; (III) Provision of study materials or patients: J Chen, Y Le, H Shi, S Ye; (IV) Collection and assembly of data: W Cui, Y Deng; (V) Data analysis and interpretation: B Huang, X Chen; (VI) Manuscript writing: All authors; (VII) Final approval of manuscript: All authors.

[#]These authors contributed equally to this work.

Correspondence to: Rongde Xu, MD. Department of Interventional Radiology, Guangdong Provincial People's Hospital (Guangdong Academy of Medical Sciences), Southern Medical University, No. 106 Zhongshan 2nd Road, Guangzhou 510080, China. Email: xurongde@gdph.org.cn; Jing Li, MD. Department of Pulmonary and Critical Care Medicine, Guangdong Provincial People's Hospital (Guangdong Academy of Medical Sciences), Southern Medical University, No. 106 Zhongshan 2nd Road, Guangzhou 510080, China; Medical School, Kunming University of Science and Technology, Department of Pulmonary and Critical Care Medicine, The First People's Hospital of Yunnan Province, Kunming, China. Email: dr.lijing@gdph.org.cn.

Background: Robotic technologies have promising applications in computed tomography (CT)-guided puncture. However, nodule-surrogate models can be difficult to develop for relevant studies, and thus the accuracy of optical navigation robot-assisted puncture remains unclear. This study aims to evaluate a starch mixture (the starch group) and a copper particle nodule-surrogate model (the particle group) and to compare the accuracy of optical navigation robot-assisted puncture (the robot group) with traditional CT-guided manual puncture (the manual group) using swine liver and kidneys.

Methods: The study was approved by the institutional animal care and use committee. *Ex vivo* and *in vivo* studies of three swine liver and kidney samples using nodule surrogates were imaged by CT scan to assess the accuracy of the starch and particle groups. In an *in vivo* study of six swine, 24 punctures made by the robot and manual groups were performed using copper particle nodule-surrogate targets in the liver and kidneys under CT guidance. The accuracy of insertion was evaluated with a 5.0-mm margin. The needle insertion time, level of radiation exposure, and complications were evaluated.

Results: In the first experiment, all nodule surrogates were easily visible on the CT images. However, other aspects of the starch group (one starch overflow, one starch dispersion event, and one air embolism) were inferior to those of the particle group. In experiment 2, the accuracy of needle insertion in the robot group (3.71±1.34 mm) was higher than in the manual group (11.89±9.59 mm) (P<0.001). The needle insertion time and level of radiation exposure were superior in the robot group compared to the manual group. Complications were similar between the two groups.

Conclusions: The particle method may be superior to the starch method. The robot group was more accurate than the manual group, and the occurrence of complications was similar.

Keywords: Robot-enhanced procedures; puncture; nodule model; liver; kidney

Submitted Sep 29, 2024. Accepted for publication Mar 25, 2025. Published online Jun 03, 2025.
doi: 10.21037/qims-24-2100
View this article at: https://dx.doi.org/10.21037/qims-24-2100

Introduction

Computed tomography (CT) image-guided minimally invasive interventional procedures such as percutaneous puncture needle biopsy and local tumor ablation are widely used in the treatment of primary and metastatic tumors (1-3). In the process of puncture, multiple scanning and image collection are required to determine the relationship between the path of the puncture needle and the target lesion. However, the accuracy of percutaneous punctures is a function of the judgment of the radiologist in traditional CT-guided manual punctures. Especially for small lesions, the direction and depth of the puncture needle may need to be adjusted several times, leading to the patients being at higher risk of repeated radiation exposure (4).

To reduce the amount of necessary needle adjustment and increase the success rate with a single puncture, various robotic-assisted navigation systems as well as manually operated electromagnetic and optical navigation systems have been developed. Compared to the traditional CT-guided manual methods, electromagnetic and robotic systems have the advantages of higher accuracy, shorter operation time, and less radiation exposure (5,6). However, electromagnetically guided puncture systems are affected by metal or other magnetic disturbances, and the magnetic field is easily interfered with (7). Optically navigated puncture systems can track the markers in real-time and guide the orientation and depth of needle insertion, thereby improving accuracy (8-10). In our previous study, a robot-assisted puncture system using optical guidance displayed advantages in the puncture of lung nodules (11), but their application in the puncture of the liver and kidney has not yet been explored.

The development of robot-assisted puncture systems for the liver and kidney has been hampered by the lack of tumor-bearing models or practical surrogates for large animal studies. Historically, pseudotumor models can be difficult to develop and thus are impractical for studies related to image-guided therapy for the liver, kidney, and other solid organs due to the time required for preparation and the viscoelastic properties of the organs (12). A previous study used tungsten balls as suitable substitutes (8). We have developed an ioversol-starch mixture that was previously applied as a lung nodule surrogate (11). However, the ability of such as starch mixture to form nodules in the liver and kidneys is unknown. Therefore, in this study, we compared the properties of two materials (a starch mixture and copper particles) to create nodule models and examined the accuracy of optical navigation robot-assisted puncture with traditional CT-guided manual puncture in *ex vivo* and *in vivo* analyses of the swine liver and kidney.

Methods

Experiments were performed under a project license (No. KY2024-208-01) granted by the Institutional Animal Care and Use Committee of Guangdong Provincial People's Hospital. All experiments were designed and performed in compliance with the general guidelines provided by the National Institutes of Health for the care and use of laboratory animals (13). All authors had complete control over the experimental data and were not involved with the company that manufactured the robot. The study comprised one *ex vivo* and two *in vivo* experiments (*Figure 1*).

Robotic system

An optical navigation robot-assisted puncture system (Wuerzburg Dynamic, Shenzhen, China) was composed of a hardware station, a navigation station, a guide, optical markers, and puncture navigation software (*Figure 2*). Briefly, the hardware station included two touch screens, an optical tracking system, and a high-performance computer for human-computer interaction and optical measurements. The navigation station comprised a multi-axis robotic arm designed for automatic punctures. The navigation software, installed on a computer, facilitates CT image processing, puncture path planning, and control of the robotic arm. A guide attached to the robotic arm directs the puncture needles. Optical markers are affixed to the skin surface of the experimental animals (swine) to track the motion of the puncture position. This robotic system was not yet commercially available.

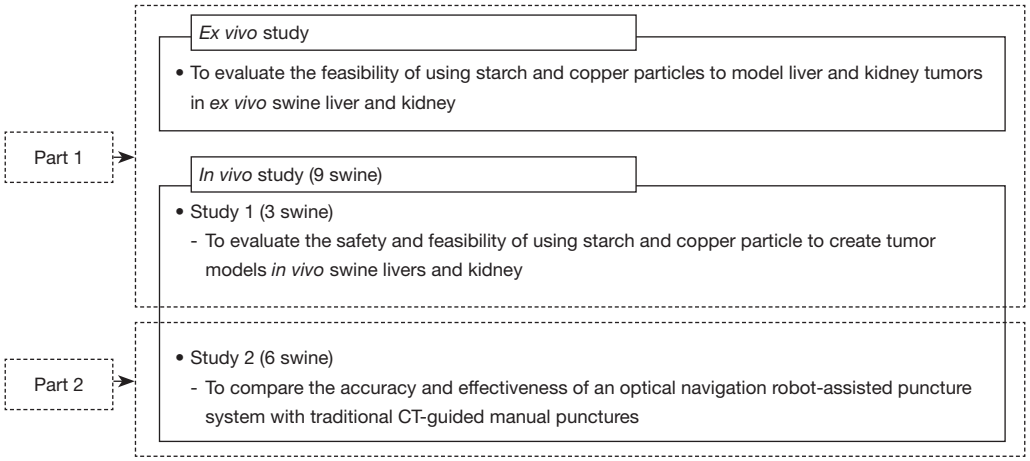

Figure 1 Flowchart showing the experimental study protocol. CT, computed tomography.

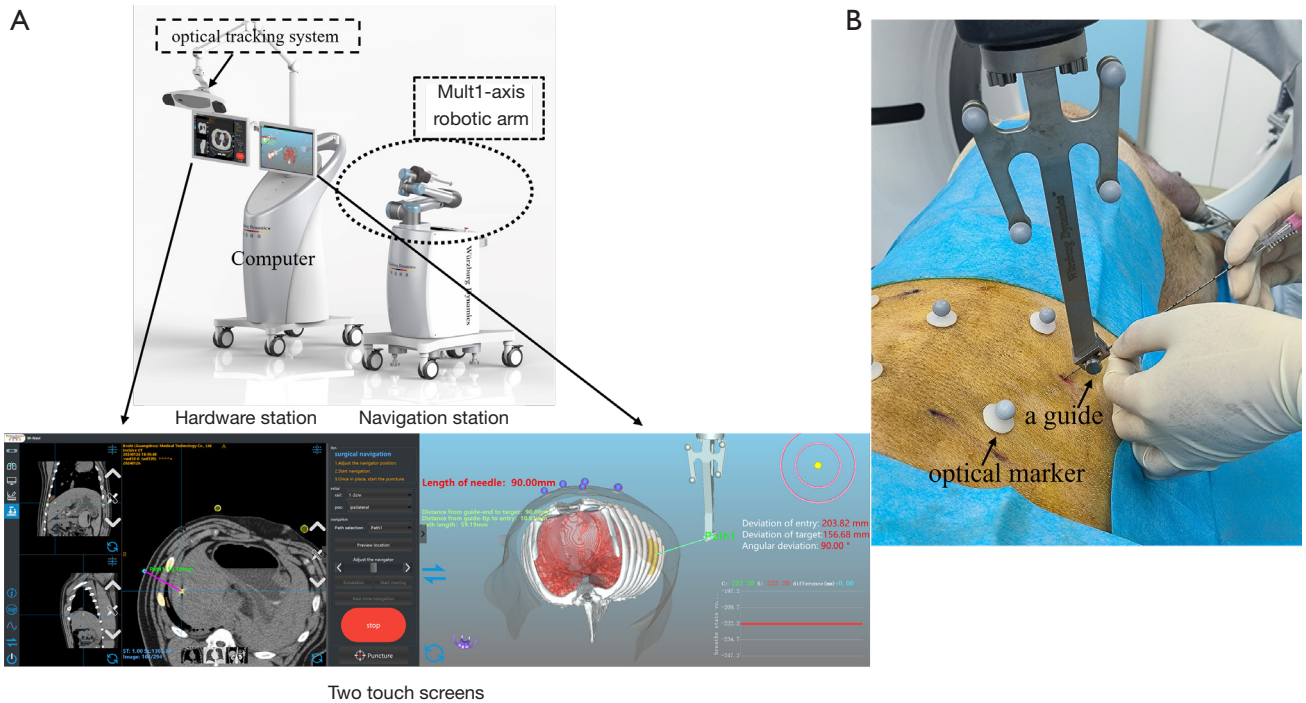

Figure 2 Optical navigation robot-assisted puncture system. The system contained a hardware station, a navigation station, a guide, optical markers, and puncture navigation software.

Part 1: creating nodule models

Ex vivo study: exploring the capabilities of starch and copper particle nodule models

Freshly harvested swine kidneys and livers were purchased from local markets, and the ioversol-starch mixture and copper particles were prepared and injected into the animal livers and kidneys to create the surrogate nodule models. Puncture success is defined as the spatial vector length between the target edge and the needle tip being less than or equal to 5 mm (8-10). Given this criterion, we selected copper particles to create the nodule model. The copper particles have dimensions of 1.0 mm × 4.0 mm. Although higher puncture accuracy is desirable, lesions smaller than

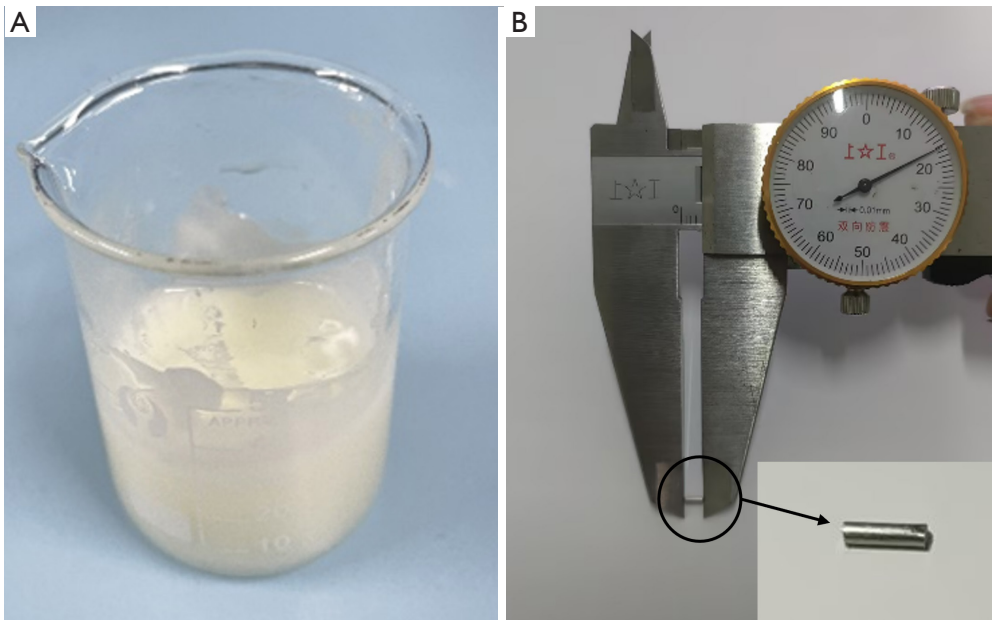

Figure 3 The nodule models with starch and copper particles. (A) Ioversol starch mixture. (B) Copper particle, 1.0 mm × 4.0 mm.

5 mm are generally not subjected to puncture operations in clinical practice. Previous studies (9,10) have used copper particles to create nodule models and have proven their feasibility. In conclusion, we chose copper particles to create the nodule model. The isolated swine liver and kidneys were placed in a basin under a CT machine (Incisive CT Power; Philips, Amsterdam, Netherlands).

For the nodule model using starch (*Figure 3A*), 10 mL of the non-ionic iodinated contrast agent ioversol was mixed with 10 mL of a 50% aqueous starch solution to create an ioversol–starch mixture. The optimal concentration of starch was assessed by injecting different concentrations of the mixture (25–75%) into *ex vivo* swine livers, and a concentration of 50% resulted in a mixture that was easily injected and that formed firm, palpable nodules in the liver parenchyma. A 1 mL syringe was used to obtain 0.5, 1.0, and 1.5 mL of the ioversol starch mixture, and each dose of starch was injected at five points into the isolated swine liver or kidney. A total of 30 starch model injections were performed.

For the nodule model using copper (*Figure 3B*), copper particles (size: φ1.0 mm × 4.0 mm) were obtained by cutting a copper wire with a diameter of 1.0 mm at equidistant points (4 mm).

For the starch group, the starch mixture was injected at 20 ℃ into isolated swine livers and kidneys at numerous sites. The maximum liver or kidney tissue depth was 5 to 15 mm. The position of the model was determined by CT scanning after implantation, and the perpendicular distance between the model and the surface of the isolated swine liver and kidney, the long axis, short axis, thickness, and volume of the starch model were recorded. The volume was calculated by the formula for an ellipsoidal (14): [1/6 π * (long axis) * (short axis) * (thickness)]. The relationship between the injected starch amount and the nodule model volume was analyzed. For the particle group, an 18G coaxial needle (BN-MAR-1; Promisemed, Hangzhou, China) was used to implant the copper particles in the isolated swine liver and kidney, and a total of 10 models were performed. The maximum liver or kidney tissue depths were the same as those of the starch group.

The visualization ability of all nodule surrogates was evaluated by CT scans, and the results were classified as invisible or visible. The shape and artifacts of nodule surrogates in the CT axis images were recorded. The shapes of the nodule models on the CT axis were classified as round, oval, rectangular, or irregular. The artifacts of nodule surrogate models on the CT scans were classified as no artifacts, small artifacts, and obvious artifacts. The experimental data underwent triple measurement averaging for accuracy by several blinded authors (R.X., X.C. two interventional radiologists with 20 and 32 years

of experience, respectively, in CT-guided intervention) to evaluate the robustness and ensure the reliability of the results. The imaging capabilities of the nodule surrogate models were immediately investigated using CT less than 15 minutes after creation in both groups.

In vivo study

The *in vivo* study consisted of two experiments. In part 1, three swine were used to explore the feasibility and safety of using starch and copper particles to create nodule models by optical robot-assisted navigation system. In part 2, six swine were used to compare the accuracy of optical navigation robot-assisted punctures with traditional CT-guided manual punctures using swine liver and kidney. A professional radiologist (W.C., with 10 years of experience in CT-guided intervention) performed all punctures and modeling operations to minimize potential variation in the procedures.

The entire optical navigation robot-assisted puncture process using the robotic system was illustrated by the following four steps (11). Step 1: system initialization to three-dimensional (3D) reconstruction of the liver and kidney. The CT images were imported into the navigation system, and the three-dimensional reconstructed according to the images. Step 2: puncture path planning to ensure a safe and unobstructed trajectory. Step 3: operation optical robot-assisted navigation to guide the device along the predetermined path with proper orientation toward the planned puncture trajectory. The patient coordinate system is registered to the world coordinate system by rigid registration of six body surface optical markers. Step 4: Puncture by the interventional radiologist.

Nine domestic female swine (mean weight, 70 kg) were included in this study. The experimental animals were intramuscularly injected with tiletamine hydrochloride (5 mg/kg) and atropine sulfate (0.08 mg/kg). The skin of the abdomen and back was prepared, and a urinary tube was inserted. Meanwhile, a vein injection needle was placed in the ear marginal vein to establish a vein passage, and propofol was slowly injected until the animals entered a state of tracheal intubation. Endotracheal intubation was performed after successful induction. Mechanical ventilation was maintained after the endotracheal intubation. The respiratory parameters were set at a tidal volume of 500 and a respiratory rate of 15, and gas anesthesia (isoflurane) was used to maintain animal anesthesia. Vital parameters such as pulse blood pressure, O_2 saturation, end-tidal CO_2, and body temperature were monitored throughout the procedure. After the experiment, the swine were sacrificed by intravenous injection of potassium chloride under general anesthesia.

Part 1: exploring the feasibility and safety of nodule models using starch and copper particles

Twelve starch or copper particle nodule-surrogate models were created in three swine (eight lesions per swine, with four per liver and two per kidney), with each nodule model being separated by at least 20 mm under the robot-assisted puncture system and CT guidance. The location of the nodule was determined by a CT scan performed by a professional interventionalist. The optical robot-assisted navigation system was then registered based on the CT scan and navigated to the position where the nodule would be placed. The amount of starch injected was set at 0.5 ml according to the above *ex vivo* study. The order of two groups of starch (the Starch group) or copper particles (the Particle group) models on the same swine was randomly determined by flipping a coin.

After the nodule models were implanted, the swine were ventilated for three minutes before the CT scan. The swine were then ventilated for five minutes, and a CT scan was again performed to evaluate the changes in the positions of the nodule models on the CT images by recording the perpendicular distances between the target and the organ surface and the skin surface, and the changes in the number of layers on CT images were recorded.

Safety level was assessed based on complications; these were classified into nodule surrogates or procedure-related. The complications were further classified as major or minor. If the complication altered the animal's condition, such as a sudden drop in blood pressure, it was deemed major; all others were defined as minor (8). The definition of successful creation of a nodule model was that the shape of the model was regular in the CT images and that complications were excluded during nodule modeling (14-17).

Part 2: comparing the accuracy and safety of optical navigation robot-assisted puncture with traditional CT-guided manual puncture in copper particle nodule models

Following the results of *in vivo* study 1, copper particles were used to create the nodule surrogates. First, an 18-gauge coaxial needle was robotic-assisted inserted into the target location using CT guidance, followed by the placement of 48 copper particles as targets. The experiment used six swine (eight models per swine, with four per liver and two per kidney).

The subjects for the nodule model were divided into two groups with a 1:1 ratio in a randomized manner based on a

coin-flip method. Within each individual swine, four nodule model punctures were performed using the optical robot-assisted system, while another four were performed using the traditional CT-guided manual method. The techniques for the robotic procedure were similar to those described in the *in vivo* study. For the manual puncture procedures, CT images were used to verify the position; if necessary, the needle was repositioned and checked again for accuracy by CT. "Accurate" was defined as a position within a 5.0-mm margin between the tip of the needle and the target. The maximum number of needle adjustments permitted was three. The trial was considered a puncture failure if the number of adjustments needed exceeded three.

The primary outcome, needle insertion accuracy, was defined as the length of the spatial vector between the target edge and the needle tip as viewed on the post-procedure CT images. The secondary outcomes were the single puncture success rate, the accuracy of skin insertion points, the needle insertion time, the second puncture success rate, needle adjustment, needle-tract length, CT scan count, the dose-length product (radiation exposure), and complications. The distance between the target and the needle tip was calculated with the Pythagorean theorem, using the x, y, and z coordinates of the coronal, sagittal, and plane sections on the CT images, respectively. The single puncture success rate was defined as one needle puncture success. The accuracy of insertion points was defined as the distance between the planned and actual insertion points. Needle insertion time was defined as the time interval between the start and the confirmation of the last puncture success on CT images. The second puncture success rate was defined as puncture success within two attempts. Needle adjustment was defined as the time needed for additional punctures. Complications were classified into procedure or robot-related. The dose-length product was used to measure radiation exposure.

Statistical analysis

Numerical variables were compared using a two-sided Student's *t*-test. A P value less than 0.05 was considered statistically significant. The 95% confidence intervals (CIs) of mean differences between the two groups were estimated. Statistical analysis was performed by using SPSS software (version 26.0; IBM, Armonk, NY, USA).

Results

Part 1: creation of models for ex vivo and in vivo studies

Thirty starch and copper particle nodule-surrogate models were created for the *ex vivo* and *in vivo* experiments. All nodule surrogates were easily visible on CT images. The CT images of starch models (*Figure 4A*) and copper particles (*Figure 4B*) demonstrated the feasibility of the models. The starch nodules on the CT images were round (20/30) or oval (10/30) and approximately 10–15 mm in diameter, and artifacts were small, while the shape of copper particles on the CT images was rectangular, and any artifacts were readily apparent. In addition, the particle volume varied depending on the amount of starch; there was a linear relation between the volumes in the liver (R^2=0.636) and kidney (R^2=0.693) (*Table 1*, *Figure 4C*).

For the *in vivo* study 1, 12 nodule models of starch and copper particles were created and used in the liver and kidneys of three swine.

In the starch group, the success rate was 75% (9/12). There were two minor (*Figure 5A*,*5B*) and one major (*Figure 5C*) nodule-surrogates-related complications in the starch group. In the particle group, the success rate was 100% (12/12) (*Figure 5D*), and no nodule-surrogate-related complications occurred. No procedure-related complications were observed in either group.

There was no significant difference in the perpendicular distance to the organ surface, the perpendicular distance to the skin surface, the changes in location, or the occurrence of complications between the starch and copper particle groups (*Table 2*) (all P>0.05).

Part 2: comparing the outcomes between robot and manual groups

The results of the *in vivo* study are summarized in *Table 3*. Representative CT images from the robot group are shown in *Figure 6*. No procedure or robot-related complications were observed.

Discussion

To the best of our knowledge, this is the first study to compare two different material capabilities for the nodule surrogate models. We found that copper particles for

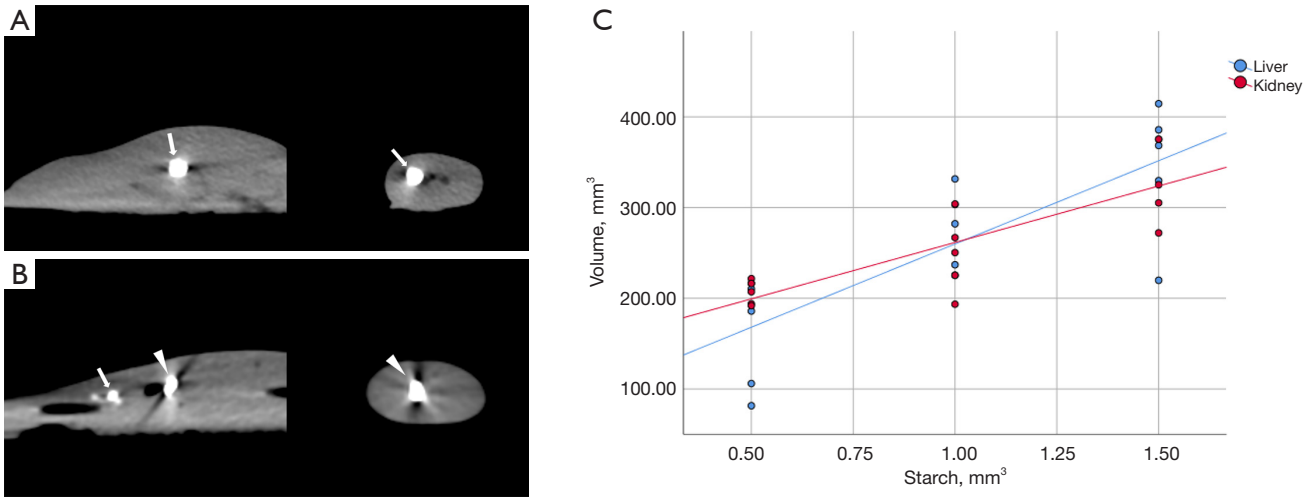

Figure 4 CT images of the nodule models with starch and copper particles in the swine liver and kidney. (A) Photographs showing CT images of starch in *ex vivo* swine liver and kidney (white arrows). (B) Photographs showing CT images of copper particles in *ex vivo* swine liver and kidney (white arrowheads) and starch in *ex vivo* swine liver (white arrow). (C) Graph showing the relationship between the starch amount and model volume. CT, computed tomography.

Table 1 The parameters of the starch nodule model

Location	Parameter	Starch (n=30)			P#
		0.5 mL (n=10)	1.0 mL (n=10)	1.5 mL (n=10)	
Liver (n=20)	Perpendicular distance (mm)	12.16±2.18	10.40±3.49	5.14±1.82	0.003
	Long axis (mm)	10.52±1.55	9.78±1.38	10.36±0.59	0.626
	Short axis (mm)	5.42±1.40	7.36±0.70	8.28±1.38	0.008
	Thickness (mm)	5.20±0.45	7.40±1.14	7.60±0.55	0.001
	Volume (mm^3)	640.21±248.88	1,103.40±178.51	1,374.47±302.86	0.002
Kidney (n=20)	Perpendicular distance (mm)	5.42±2.09	7.40±3.46	2.82±1.81	0.046
	Long axis (mm)	8.70±0.97	9.92±1.56	11.36±0.47	0.008
	Short axis (mm)	6.22±0.81	6.42±1.48	8.60±1.80	0.039
	Thickness (mm)	7.40±0.89	8.00±2.92	6.60±0.89	0.501
	Volume (mm^3)	824.56±52.85	991.97±167.17	1,322.33±179.90	0.001

Data are presented as mean ± standard deviation. #, P is the difference between the three groups of starch.

creating nodule models were superior to starch. Optical navigation robot-assisted punctures exhibited higher accuracy compared to traditional CT-guided manual punctures, and the complication rate was similar.

In our previous study, we successfully used starch for modeling lung nodules in swine, but the present study has demonstrated that such starch models for swine liver and kidney are unsatisfactory (11). Using starch as a nodule surrogate has the following advantages. Firstly, starch is cheap and easy to obtain, and starch is easy to implant; secondly, the size of the nodule starch models can be adjusted by varying the injected quantity; finally, compared

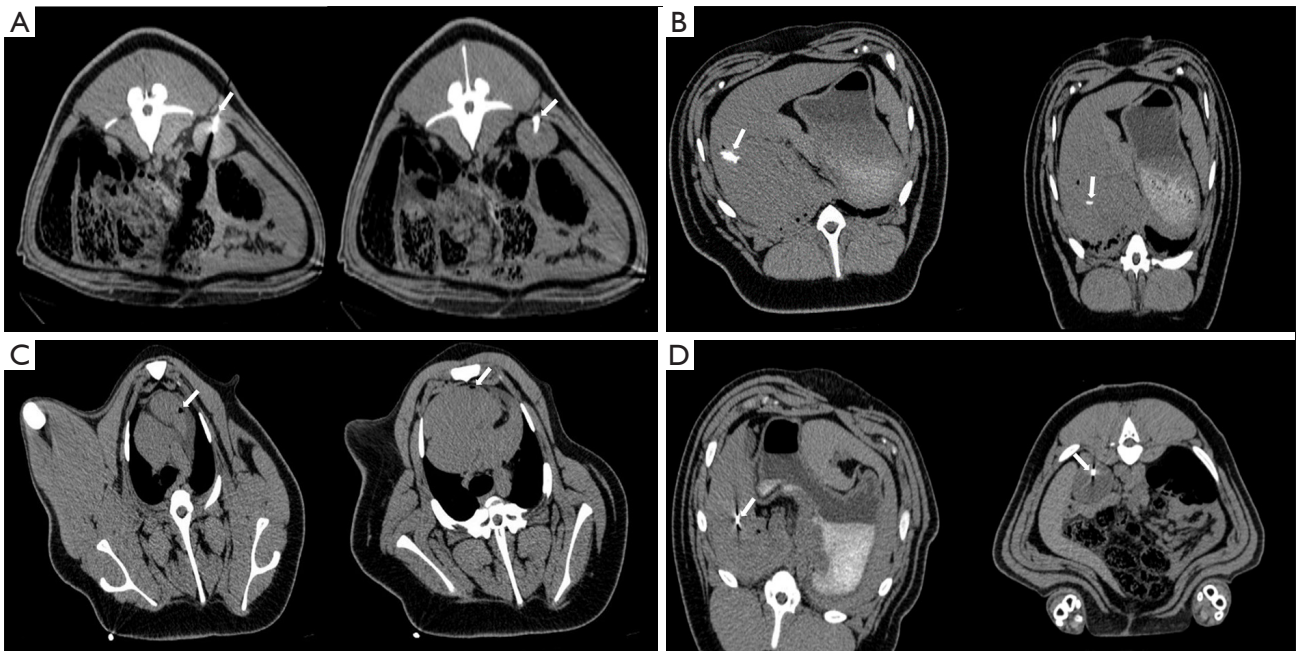

Figure 5 CT images of nodule model of starch and copper particle *in vivo* swine liver and kidney. (A) Photographs showing the starch overflow into the organ surface in the kidney after injection (white arrows). (B) Photographs showing the starch diffusing and entering the blood vessels after the injection in the liver (white arrows). (C) Photographs showing the CT images revealed two air bubbles in the cardiac vessels of the swine (white arrows). (D) Photographs showing CT images of copper particles in the swine liver and kidney (white arrows). CT, computed tomography.

Table 2 The results of the nodule models of starch and copper particles

Location	Parameter	Starch (n=12)	Copper particles (n=12)	P
Liver (n=12)	Perpendicular distance to the skin surface (mm)	48.40±12.81	62.98±11.45	0.064
	Perpendicular distance to organ surface (mm)	17.10±8.90	22.97±8.81	0.278
	Changes in location (mm)	2.50±3.21	3.83±1.33	0.369
	Complication	2/6 (33.3%)	0/6 (0)	0.175
Kidney (n=12)	Perpendicular distance to the skin surface (mm)	53.93±11.72	58.13±13.51	0.578
	Perpendicular distance to organ surface (mm)	13.63±3.38	10.95±1.63	0.111
	Changes in location (mm)	2.50±1.76	2.83±2.71	0.806
	Complication	1/6 (16.7%)	0/6 (0)	0.363

Data are presented as mean ± standard deviation.

to copper particles, the nodule models with starch allow for biopsies to verify the puncture outcome (11). Nevertheless, there were two minor and one major nodule-surrogate-related complications in the starch group. Air embolism may lead to death, and this could be attributed to the prolonged duration of the operation. The association between air embolism and the creation of the nodule model was unclear, and starch was not observed in the cardiac vasculature of swine on the CT images. We speculate that the main reason may be that the liver and kidney are more sinus-rich organs than the air-rich lung tissue, and this affected the performance of the starch model. de Baere *et al.* (9)

Table 3 The results of the *in vivo* study 2 with a copper particle nodule model

Location	Parameter	Robot insertion (n=24)	Manual insertion (n=24)	P
Liver (n=24)	Needle insertion accuracy (mm)	4.01±1.65	8.83±4.17	0.002
	Single puncture success rate	100% (12/12)	58.33% (7/12)	0.017
	Insertion points accuracy (mm)	2.56±1.21	6.38±5.85	0.038
	Needle insertion time (min)	3.50±0.67	7.33±5.00	0.023
	Second puncture success rate	100% (12/12)	75% (9/12)	0.082
	Needle adjustments	0	0.67±0.89	0.025
	Needle-tract length (mm)	74.25±17.00	69.92±14.10	0.503
	CT scan count	2	2.67±0.89	0.025
	Dose-length product (mGy·cm)	992.76±171.03	1,356.22±599.62	0.065
Kidney (n=24)	Needle insertion accuracy (mm)	3.40±0.91	14.96±12.42	0.008
	Single puncture success rate	100% (12/12)	33.33% (4/12)	0.001
	Insertion points accuracy (mm)	2.91±1.36	6.43±6.47	0.091
	Needle insertion time (min)	3.92±0.90	8.00±4.22	0.007
	Second puncture success rate	100% (12/12)	66.67% (8/12)	0.039
	Needle adjustments	0	1.00±0.85	0.002
	Needle-tract length (mm)	70.56±13.16	75.97±23.79	0.500
	CT scan count	2	3.00±0.85	0.002
	Dose-length product (mGy·cm)	1,102.12±151.17	1,652.39±512.04	0.003

Data are presented as mean ± standard deviation. CT, computed tomography.

used metal particles to create a kidney nodule model. All the nodule models using metal particles were successfully created (8/8). Guiu *et al.* (10) used metal particles (1 mm × 5 mm) to create liver nodule models. The success rate was 96.7% (64/66). Our study showed that the utilization of copper particles for the creation of liver and kidney nodule models was both safe and feasible, and the success rate was similar to those of the above studies. Hence, despite the inability to use copper particles for biopsy purposes, this method remains ideal for liver and kidney nodule model creation.

In this study, the optical navigation robot-assisted puncture system exhibited higher accuracy and effectiveness compared to traditional CT-guided manual puncture. The robotic system facilitated needle insertion with a higher single puncture success rate and greater accuracy than the manual method, requiring fewer adjustments, reducing operation time, and minimizing radiation exposure. These advantages could be due to several factors. First, the needle-tract length of the navigation device was planned as an integer, and thus it was easy to determine the needle depth, while the manual puncture method was usually non-integral. Second, the navigation device provided a stable angle to facilitate the puncture. Third, the path planning of the navigation device was unaffected by the patient's body position. Finally, the accuracy of puncture was easily affected by the subjective factors involving individual doctors. A previous study showed that the single puncture accuracy was 80.5% (29/36) without complications (10). de Baere *et al.* reported the single puncture rate of robotic assistance for percutaneous needle insertion was 100% (8/8); the needle insertion accuracy was 2.80±2.73 mm, and two hematoma complications (2/8) occurred (9). These results were similar to ours. In our study, the robot-assisted system reduced the number of needle insertion adjustments due to incorrect direction or depth, thereby shortening the puncture time and decreasing the risks of bleeding and radiation exposure (18). Before the puncture, a coaxial puncture path based on the nodule model was planned, coaxial puncture needles

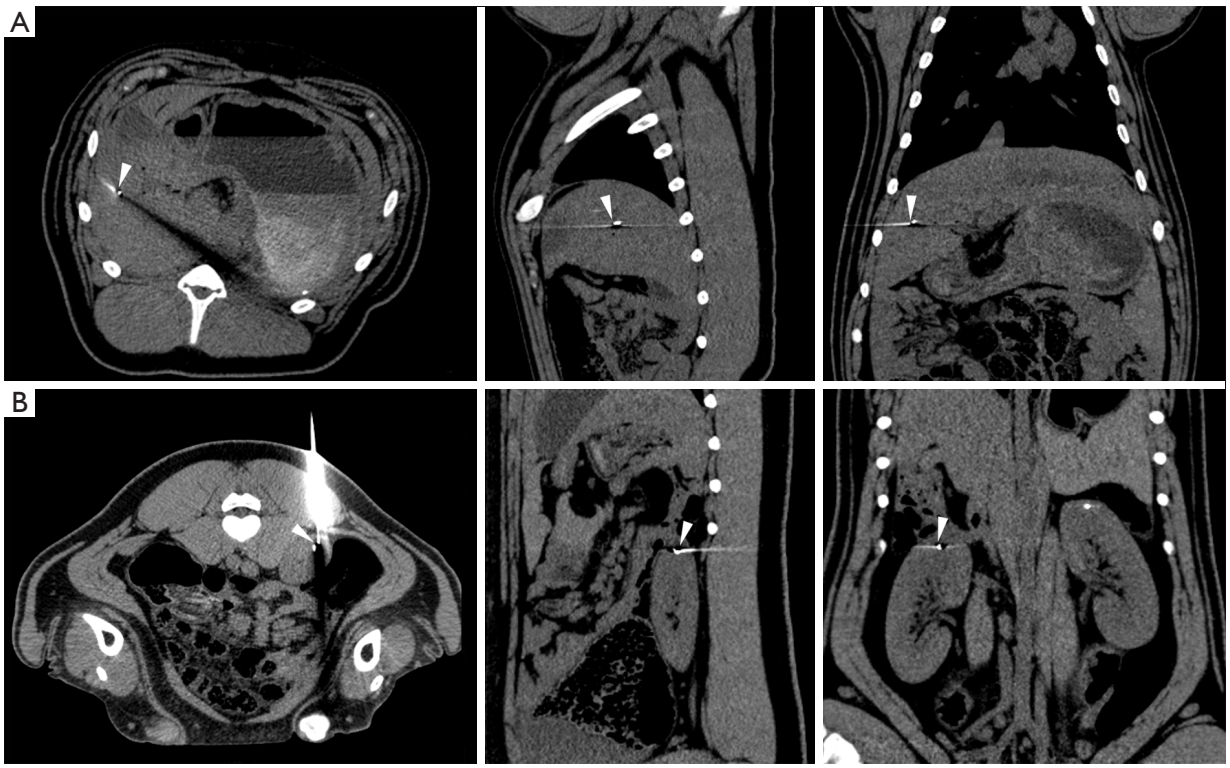

Figure 6 Liver and kidney puncture in place. (A) Photographs showing CT images of the copper particles reached by the tip of the needle in the swine liver, in the plane, sagittal, and coronal positions, respectively (white arrowheads). (B) Photographs showing the CT images of the copper particles reached by the tip of the needle in the swine kidney, in the plane, sagittal, and coronal positions, respectively (white arrowheads). CT, computed tomography.

were used, and the number of punctures was minimized (18,19). These measures also reduced the incidence of complications. The primary disadvantage of optical systems is that the camera and optical markers can be obstructed. Although electromagnetic navigation systems are not limited by light blocking, their performance can be affected by metal or other magnetic disturbances (7). A retrospective study showed that the needle insertion accuracy through electromagnetic navigation was 8.3±3.7 mm (20). Compared to our study, the needle insertion accuracy differed due to the electromagnetic navigation system's susceptibility to magnetic interference. Moreover, the robot-assisted system could provide specific guidance for young doctors with limited experience in puncture biopsy, thereby offering beginners more experience and greater confidence. Experienced interventional radiologists and puncture navigation robots both have their unique advantages and are not in conflict (21). Guiu *et al.* (10) compared the accuracy of needle insertions performed by three experienced interventional radiologists (with at least 10 years of experience in liver needle biopsy) and by a veterinarian who was a complete novice in image-guided needle insertion. Interestingly, the accuracy did not differ between the novice and experienced operators. We will continue to conduct relevant research to explore deeper integration and collaboration between experienced interventional radiologists and puncture navigation robots, with the goal of achieving better medical outcomes.

There are several limitations to our study. First, the application of deep sedation and general anesthesia in animal experiments can weaken the influence of respiratory movement on puncture accuracy, a situation that differs from the local anesthesia used in clinical practice. Second, the distribution of liver nodule models may not be random, and the effects of puncture depth and complex sites were not evaluated. Third, the nodule models used in this study were not actual tumors. Moreover, the study did not assess the impact of robot-assisted systems on novice and

experienced interventional radiologists. Finally, very small lesions are generally not punctured in actual clinical work, and for lesions that are close to important organs or large blood vessels, it is necessary to maintain high precision.

Conclusions

In conclusion, the use of copper particles as nodule models may be superior to using starch. Optical navigation robot-assisted puncture exhibited higher accuracy compared to the traditional CT-guided manual puncture, and the two methods showed similar rates of complications.

Acknowledgments

None.

Footnote

Funding: This study was supported by 2024 Basic and Applied Basic Research Theme (Outstanding Doctoral "Continuing Sail" Project) (No. 2024A04J2459), the National Natural Science Foundation of China (No. 82102163), and the National Key Research and Development Program (project No. 2023YFC2507104).

Conflicts of Interest: All authors have completed the ICMJE uniform disclosure form (available at https://qims.amegroups.com/article/view/10.21037/qims-24-2100/coif). The authors have no conflicts of interest to declare.

Ethical Statement: The authors are accountable for all aspects of the work in ensuring that questions related to the accuracy or integrity of any part of the work are appropriately investigated and resolved. Experiments were performed under a project license (No. KY2024-208-01) granted by the Institutional Animal Care and Use Committee of Guangdong Provincial People's Hospital. All experiments were designed and performed in compliance with the general guidelines provided by the National Institutes of Health for the care and use of laboratory animals.

References

1. Li J, Liu G, Xie X, Zhang D, Zheng R, Yang H, Zhong H, Dai G, Yu J, Liang P. Outcomes Following Different Thermal Ablation Strategies in Patients with Unresectable Colorectal Liver Metastases. Radiology 2023;308:e223135.
2. Lee GY, Chung JH, Cho S, Han YB, Park YM, Kim HJ, Song MJ, Kwon BS, Lim SY, Lee YJ, Park JS, Cho YJ, Yoon HI, Lee JH, Lee CT, Kim YW. Impact of Preoperative Diagnostic Biopsy Procedure on Spread Through Airspaces and Related Outcomes in Resected Stage I Non-Small Cell Lung Cancer. Chest 2022;162:1199-212.
3. Murphy MC, Wrobel MM, Fisher DA, Cahalane AM, Fintelmann FJ. Update on Image-Guided Thermal Lung Ablation: Society Guidelines, Therapeutic Alternatives, and Postablation Imaging Findings. AJR Am J Roentgenol 2022;219:471-85.
4. Wiener RS, Schwartz LM, Woloshin S, Welch HG. Population-based risk for complications after transthoracic needle lung biopsy of a pulmonary nodule: an analysis of discharge records. Ann Intern Med 2011;155:137-44.
5. Zhao Y, Mei Z, Luo X, Mao J, Zhao Q, Liu G, Wu D. Remote vascular interventional surgery robotics: a literature review. Quant Imaging Med Surg 2022;12:2552-74.
6. Smakic A, Rathmann N, Kostrzewa M, Schönberg SO, Weiß C, Diehl SJ. Performance of a Robotic Assistance Device in Computed Tomography-Guided Percutaneous Diagnostic and Therapeutic Procedures. Cardiovasc Intervent Radiol 2018;41:639-44.
7. Sorriento A, Porfido MB, Mazzoleni S, Calvosa G, Tenucci M, Ciuti G, Dario P. Optical and Electromagnetic Tracking Systems for Biomedical Applications: A Critical Review on Potentialities and Limitations. IEEE Rev Biomed Eng 2020;13:212-32.
8. Hiraki T, Kamegawa T, Matsuno T, Sakurai J, Kirita Y, Matsuura R, Yamaguchi T, Sasaki T, Mitsuhashi T, Komaki T, Masaoka Y, Matsui Y, Fujiwara H, Iguchi T, Gobara H, Kanazawa S. Robotically Driven CT-guided Needle Insertion: Preliminary Results in Phantom and Animal Experiments. Radiology 2017;285:454-61.
9. de Baere T, Roux C, Noel G, Delpla A, Deschamps F, Varin E, Tselikas L. Robotic assistance for percutaneous

needle insertion in the kidney: preclinical proof on a swine animal model. Eur Radiol Exp 2022;6:13.
10. Guiu B, De Baère T, Noel G, Ronot M. Feasibility, safety and accuracy of a CT-guided robotic assistance for percutaneous needle placement in a swine liver model. Sci Rep 2021;11:5218.
11. Li J, Su L, Liu J, Peng Q, Xu R, Cui W, Deng Y, Xie W, Huang B, Chen J. Optical navigation robot-assisted puncture system for accurate lung nodule biopsy: an animal study. Quant Imaging Med Surg 2023;13:7789-801.
12. van Vledder MG, Assumpcao L, Munireddy S, Sehgal K, Boctor EM, Choti MA. Development of hepatic pseudotumors for image-guided interventional and surgical research in a large animal model. J Vasc Interv Radiol 2011;22:1452-6.
13. Committee for the Update of the Guide for the Care and Use of Laboratory Animals IfLAR, Division on Earth and Life Studies, National Research Council. Guide for the care and use of laboratory animals. 8th ed. Washington, DC: National Academies Press; 2011.
14. Kawai T, Kaminou T, Sugiura K, Hashimoto M, Ohuchi Y, Adachi A, Fujioka S, Ito H, Nakamura K, Ihaya T, Ogawa T. Percutaneous radiofrequency lung ablation combined with transbronchial saline injection: an experimental study in swine. Cardiovasc Intervent Radiol 2010;33:143-9.
15. Prud'homme C, Teriitehau C, Adam J, Kyaw Tun J, Roux C, Hakime A, Delpla A, Deschamps F, de Baere T, Tselikas L. Lung microwave ablation - an in vivo swine tumor model experiment to evaluate ablation zones. Int J Hyperthermia 2020;37:879-86.
16. Kawai T, Kaminou T, Sugiura K, Hashimoto M, Ohuchi Y, Adachi A, Fujioka S, Ito H, Nakamura K, Ogawa T. Creation of a tumor-mimic model using a muscle paste for radiofrequency ablation of the lung. Cardiovasc Intervent Radiol 2009;32:296-302.
17. Xin N, Wu X, Chen Z, Wei R, Saito Y, Lachkar S, Salvicchi A, Fumimoto S, Drevet G, Xu Z, Huang K, Tang H. A new preoperative localization of pulmonary nodules guided by mixed reality: a pilot study of an animal model. Transl Lung Cancer Res 2023;12:150-7.
18. Cornelis F, Takaki H, Laskhmanan M, Durack JC, Erinjeri JP, Getrajdman GI, Maybody M, Sofocleous CT, Solomon SB, Srimathveeravalli G. Comparison of CT Fluoroscopy-Guided Manual and CT-Guided Robotic Positioning System for In Vivo Needle Placements in Swine Liver. Cardiovasc Intervent Radiol 2015;38:1252-60.
19. Heerink WJ, Ruiter SJS, Pennings JP, Lansdorp B, Vliegenthart R, Oudkerk M, de Jong KP. Robotic versus Freehand Needle Positioning in CT-guided Ablation of Liver Tumors: A Randomized Controlled Trial. Radiology 2019;290:826-32.
20. Banovac F, Tang J, Xu S, Lindisch D, Chung HY, Levy EB, Chang T, McCullough MF, Yaniv Z, Wood BJ, Cleary K. Precision targeting of liver lesions using a novel electromagnetic navigation device in physiologic phantom and swine. Med Phys 2005;32:2698-705.
21. Barral M, Razakamanantsoa L, Cornelis FH. How to further train medical students in Interventional Radiology? Diagn Interv Imaging 2021;102:9-10.

Cite this article as: Cui W, Deng Y, Chen J, Le Y, Shi H, Ye S, Huang B, Chen X, Li J, Xu R. CT-guided needle insertion with an optical navigation robot-assisted puncture system: *ex vivo* and *in vivo* experimental studies in the liver and kidneys. Quant Imaging Med Surg 2025;15(6):5114-5125. doi: 10.21037/qims-24-2100

